~~A Moored Array Observation Dataset for Air-Sea Surface~~MASCS 1.0: Synchronous atmospheric and ~~Ocean~~oceanic data from a cross-shaped moored array in the ~~Northern~~northern South China Sea during 2014–2015 ~~(MASCS 1.0)~~

Han Zhang[1,2,3~~*~~], Dake Chen[1,2,4], Tongya Liu[1,2], Di Tian[1], Min He[2], Qi Li[2], Guofei Wei[6,7], Jian Liu[2,5]

~~Correspondence: Han Zhang (zhanghan@sio.org.cn)~~

[1] State Key Laboratory of Satellite Ocean Environment Dynamics, Second Institute of Oceanography, Ministry of Natural Resources, Hangzhou 310012, China

[2] Southern Marine Science and Engineering Guangdong Laboratory (Zhuhai), Zhuhai 519082, China

[3] State Key Laboratory of Marine Environmental Science, Xiamen University, Xiamen 361102, China

[4] School of Oceanography, Shanghai Jiao Tong University, Shanghai 200030, China

[5] School of Geography and Ocean Science, Ministry of Education Key Laboratory for Coast and Island Development, Nanjing University, Nanjing 210023, China

[6] Key Laboratory of Straits Severe Weather China Meteorological Administration, Fuzhou 350028, China

[7] Fujian Meteorological Observatory, Fuzhou 350028, China

Correspondence: Han Zhang (zhanghan@sio.org.cn)

Abstract. This ~~study reports~~work presents a cross-shaped moored array dataset (MASCS 1.0) ~~consisting of~~comprising five buoys and four moorings with synchronous atmospheric and oceanic data in the northern South China Sea during 2014–2015. The ~~dataset includes measurements~~atmospheric data are observed by two meteorological instruments at the buoys. The oceanic data consist of sea surface ~~meteorological data using two sets of instruments, sea surface~~ waves measured ~~by~~using a wave recorder, temperature, and salinity from the surface to a depth of 400 m, and at 10 ~~m~~ and 50 m above the ocean bottom ~~by~~using conductivity, temperature, and depth ~~(CTD)~~ recorders. It also includes currents from the surface to a depth of 850 m measured ~~by~~using acoustic Doppler current profilers ~~(ADCPs)~~ and measured at 10 ~~m~~, 50 ~~m~~, and 100 m above the floor ~~measured by~~using

设置了格式: 英语(美国)

设置了格式: 英语(美国)

带格式的: 段落间距段前: 0.5 行, 段后: 0.5 行

设置了格式: 英语(美国)

设置了格式: 英语(美国)

current meters. Additional measurements were taken for sea surface radiation, air visibility, chlorophyll, turbidity, and chromophoric dissolved organic matter at ~~Buoy~~buoy 3~~, which was~~ located at the center of the moored array. The data reveals air~~-~~–sea interactions and oceanic processes in the upper and bottom ocean, especially the transition of the air~~-~~–sea interface and ocean conditions from summer to winter monsoon ~~along with~~and the effects of six tropical cyclones on the moored array. ~~The multiscale~~Multiscale processes were also recorded, such as air~~-~~–sea fluxes, tides, internal waves, and low-frequency flows ~~were also recorded.~~. The data ~~is~~are valuable and ~~has multiple~~have many potential applications, including ~~analysis of~~analyzing the phenomena and mechanisms of air~~-~~–sea interactions and ocean dynamics~~, as well as validation and improvement of~~ and validating and improving numerical model simulations, data reanalysis, and assimilations. All the data described here are made publicly available ~~from~~at ~~https://zenodo.org/records/13827819~~https://zenodo.org/records/13925651 (Zhang et al. 2024).

1 Introduction

设置了格式: 英语(美国)

The South China Sea (SCS) is a semi-enclosed marginal sea with a deep basin, making it the largest marginal sea in the tropics, covering ~~nearly~~approximately 3.5 × 10^6 km^2. The ~~South China Sea~~SCS is also the largest marginal sea in the western Pacific~~,~~ and is known for its powerful internal tides and abundant internal waves (Alford et al., 2015). Mesoscale eddies in the SCS transport heat and salt from the Kuroshio loop near the Luzon Strait (Yang et al., 2019) and modulate sea surface fields (Tan et al., 2023). The background circulations in the SCS are cyclonic in the upper and deep layers, ~~while~~whereas they are anticyclonic in the middle layer (Cai et al., 2020). The three factors contributing to the generally cyclonic gyre in the upper ocean of the northern SCS (Jilan, 2004; Liu et al., 2008) are~~:~~ (1) quasi-seasonal wind forcing~~;~~, (2) net water transport into the SCS through the Luzon Strait~~;~~, and (3) vorticity advection from the Kuroshio. The Kuroshio carrying the northwestern Pacific water intrudes into the SCS through the Luzon Strait (Nan et al., 2015).

~~The SCS is~~Atmospheric forcing significantly ~~influenced by atmospheric forcing~~influences the SCS, such as monsoons (Chen et al., 2023; Chen et al., 2022), tropical cyclones (TCs) (Guan et al., 2024; Shan et al., 2023), and the world's strongest boreal summer quasi-biweekly oscillation (Qi et al., 2023). Marine heat waves (Wang et al., 2022) and ~~variations in~~ air~~-~~–sea heat flux variations (Song et al., 2023; Zhang, 2023) are also observed in the northern SCS. This sector features broad continental shelves and steep continental slopes, leading to complex local ocean dynamical processes. For example, breaking internal tides on the continental slope induce along-slope deep sea bottom currents (Xie et al., 2018), and cross-isobathic motion of the water column or synoptic processes (e.g., TCs) induce continental shelf waves, such as topographic Rossby (Wang et al., 2019) and Kelvin mode (Li et al., 2024) waves.

~~Owing~~Due to the complexity of air~~-~~–sea interaction and oceanic processes in the SCS, local in~~-~~ situ observations are essential to ~~uncover the~~uncovering their phenomena and mechanisms. From 2014 to 2015, a cross-shaped moored array ~~consisting of~~comprising five buoys and four moorings was deployed in the northern SCS to acquire sea surface meteorological and ~~oceanic data as well as~~ upper and near-bottom oceanic data. This study lists the details of these observations and the resulting dataset. ~~Part of this~~Some data have already been used in several studies focusing on air~~-~~–sea heat flux, ocean temperature–_salinity, and dynamical responses to tropical cyclonesTCs (Zhang et al., 2016; Zhang et al., 2018; Liu et al., 2020; Zhang, 2023),) to investigate the effect of drag coefficients on surface heat flux during typhoontyphoons (Liu et al. 2022), the influence of typhoons on the pre-existingpreexisting eddies (He et al., 2024), ocean mixing and heat flux by near-inertial waves (Hong et al. 2022; Lu et al., 2024), sea surface wind patterns (Zhang et al., 2020) and the comparison of microseismscomparing microseism signals generated by typhoons (Lin et al., 2022), the validity of numerical model simulations (Wu et al., 2020; Lim Kam Sian et al., 2020; Lu et al., 2023), and the study of deep ocean energy variability in the SCS (Quan et al., 2022). However, the full potential of this dataset has yet to be realized.

2 Moored array observations

2.1 Positions of buoys and moorings

The observation array consisted ofcomprised five buoys (B1-–B5) and four moorings (M1, M2, M4, M5) in the northern South China SeaSCS (Figs. 1 and 2), deployed from June to September 2014 and recovered from September 2014 to March 2015 (Table 1). The water depth at buoy 1 (B1) and mooring 1 (M1) was approximately 1600 m, whilewhereas the depths at the other stations were greater than 3000 m. Tropical cyclonesTCs significantly influenced the observations, as shown in (Fig. 1,), including Hagibis in June, Rammasun and Matmo in July, Kalmaegi and Fung-wong in September, and Hagupit in December. The information regarding these tropical cyclonesTCs was obtained from the China Meteorological Administration (https://tcdata.typhoon.org.cn/en/zjljsjj.html), which were deemedis more accurate for tropical cyclonesTCs affecting China (Lu et al., 2021; Ying et al., 2014). Although the designdesigns of some buoys and moorings have already been shown in previous works (e.g. studies (Zhang et al., 2016; Zhang, 2023), the designs of all the stations are redrawn to give more accurate information ofon the deployment of the instruments (Fig. 1b, Fig. 3).

Table 1 shows the locations of the observation stations as well asand their time range. The moorings (M1, M2, M4, and M5) were deployed during 8 to 10 June 8–10, 2014, and successfully recovered during 29 to 31 March 29–31, 2015 (Table 1). B1 was deployed on 19 June 19, 2014, and maintained once on 5 September 5, 2014, it. It lost contact on 15 October while did15 and was not recoverrecovered by two cruises during 23from March 23 to 4 April 4, 2015. Buoy 2 (B2) and 4 (B4) were deployed on 29 July 29 and 20 June 20, 2014, whilerespectively, and recovered on 30 March 30, 2015. B4 was maintained once on 30 July 30, 2014. Buoy 3 (B3) was deployed on 11 September, the 11, 2014. The tether of B3 snapped on 15 September 15, 2014, when typhoon Kalmaegi passed over the observation array (Zhang et al., 2016). B3 then became a drifter, initially moving northeastward with circular tracks (Fig. 2a) attributed to the rightward advection and near-inertial surface currents induced by the typhoon. B3 returned to its initial location on 21 September 21, 2014, moved eastward and turned back on 25 September 25, 2014, and followed a southwestward track thereafterafter that (Fig. 2a). B3 wasA ship recovered by a shipB3 on 17 October 17, 2014, and it was brought back to land on 21 October 21, 2014. MooredThe moored part of B3 was recovered on 31 March 31, 2015. Buoy 5 (B5) was deployed on 26 August 26, 2014, and lost contact on 11 October 11, 2014, while the. The moored part of B5 was recovered on March 31 March, 2015. The horizontal movement of the buoys was minimal during

设置了格式: 英语(美国)
设置了格式: 英语(美国)
设置了格式: 英语(美国)
带格式的: 缩进: 首行缩进: 2.5 字符

observations~~, as~~ because they primarily moved in a circular region with a radius shorter than 3 km (Figs. 2b~~–~~–e). Typhoon Kalmaegi also increased the horizontal circular movement of B1 to approximately 4 km on the northwest side on ~~15~~ September 15, which was attributed to the northwestward winds on the right-hand side of the typhoon~~ and may indicate~~, indicating that the typhoon moved the anchor of B1 ~~was~~ northwestward ~~moved by the typhoon as~~because its tether length was approximately 2 km (nearly half of 4 km~~), see~~) (Figs. 2c and 3a~~.~~).

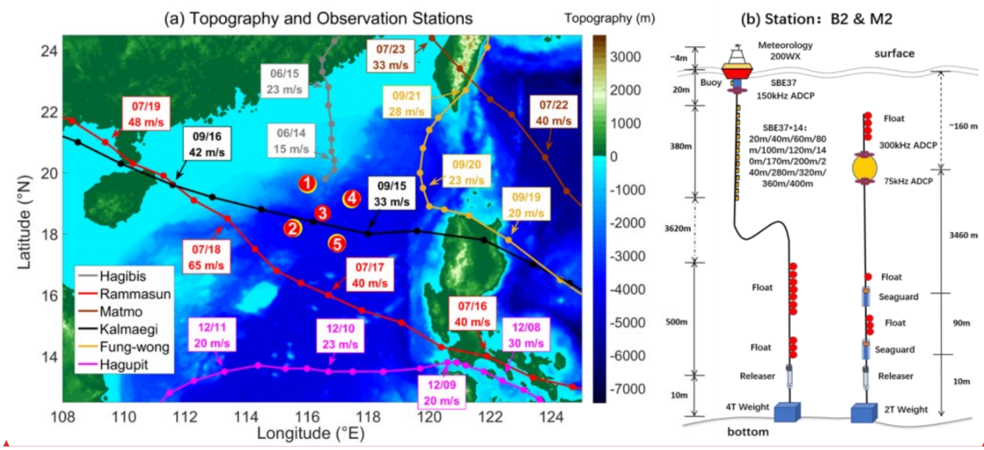

Figure 1~~:~~. **(a)**~~:)~~ Topography (m) map with the positions ~~of~~ and ~~the~~ deployed locations of the buoys (red dots) and moorings (yellow dots). **(b)** Designs of buoy 2 (B2) and mooring 2 (M2) are shown as examples~~,~~; the dot-and-dash line indicates the tether length in the middle water of the buoy, ~~while~~and the dashed line indicates the depth of the two ADCPs on the top of the mooring. ~~Tracks~~The tracks of ~~tropical cyclones~~the TCs are shown (colored lines~~), along with~~) and their positions every 6 h (dots). The text boxes indicate the dates and the sustained maximum wind speed at UTC 00:00 on each date.

设置了格式: 英语(美国)
设置了格式: 英语(美国)
设置了格式: 英语(美国)
设置了格式: 字体: 非加粗, 英语(美国)
设置了格式: 字体: 非加粗
设置了格式: 字体: 非加粗
设置了格式: 字体: 非加粗
设置了格式: 字体: 非加粗
设置了格式: 字体: 非加粗
设置了格式: 字体: 非加粗
设置了格式: 字体: 非加粗
设置了格式: 字体: 非加粗
设置了格式: 字体: 非加粗
设置了格式: 字体: 非加粗
设置了格式: 字体: 非加粗
设置了格式: 字体: 非加粗
设置了格式: 字体: 非加粗
设置了格式: 字体: 非加粗, 英语(美国)

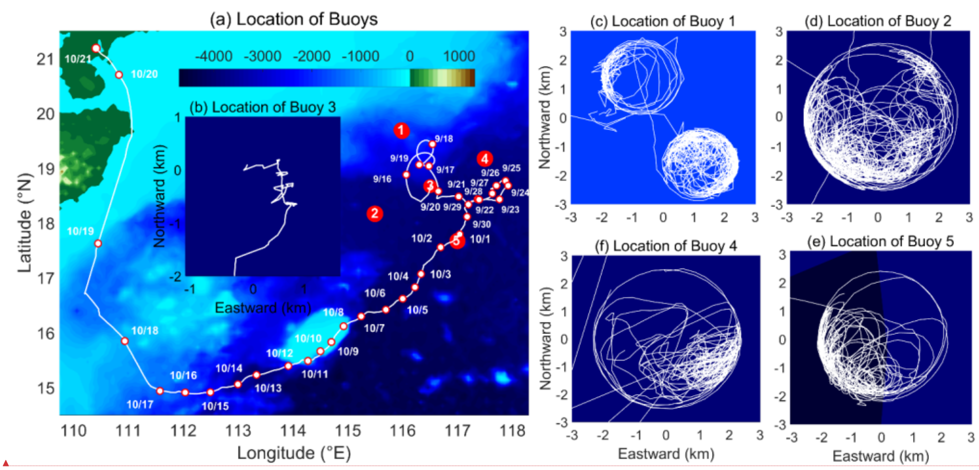

Figure 2~~:~~. **(a**~~):~~) Distributions of the buoy locations, with the track of buoy 3 (B3). **(b–e**~~):~~) Tracks of ~~buoy~~buoys 3, 1, 2, 4, and 5 (B3, B1, B2, B4, and B5) with their locations relative to their initial deployed positions in northward and eastward directions (km). ~~White~~The white lines represent the buoy tracks, ~~while~~and the white hollow dots indicate the positions of B3 every day after ~~15~~ September 15, 2014, when its tether snapped and it became a drifter.

Table 1. Information of the observation station

Station	Deployed Longitude (E)	Deployed Latitude (N)	Estimated Water Depth (m)	Time Range*
Buoy 1 (B1)	115°59’49.8”	19°40’04.8”	1625	2014.06.19–2014.10.15
Buoy 2 (B2)	115°29’53.5”	18°09’59.3”	3710	2014.07.29–2015.03.30
Buoy 3 (B3)	116°30’33.9”	18°40’40.2”	3310	2014.09.11–2014.10.17
Buoy 4 (B4)	117°30’11.4”	19°10’01.7”	3430	2014.06.20–2014.03.30
Buoy 5 (B5)	116°59’55.7”	17°39’58.8”	3930	2014.08.26–2015.03.31
Mooring 1 (M1)	116°01’17.1”	19°37’28.7”	1630	2014.06.08–2015.03.29
Mooring 2 (M2)	115°32’57.8”	18°11’29.5”	3740	2014.06.10–2015.03.30
Mooring 4 (M4)	117°27’16.8”	19°08’24.9”	3410	2014.06.09–2015.03.30
Mooring 5 (M5)	116°58’50.8”	17°42’18.1”	3930	2014.06.10–2015.03.31

*B1 ~~were~~was lost and not recovered, and the end time of B1 represents the latest time when observation data were received. Otherwise, the time range represents the deployment and recovery time for the stations.

设置了格式: 英语(美国)
设置了格式: 英语(美国)
设置了格式: 英语(美国)
设置了格式: 英语(美国)
设置了格式: 字体: 非加粗, 英语(美国)
设置了格式: 英语(美国)
设置了格式: 英语(美国)
设置了格式: 英语(美国)
设置了格式: 字体: 非加粗, 英语(美国)
设置了格式: 字体: 非加粗, 英语(美国)
设置了格式: 字体: 非加粗, 英语(美国)
设置了格式: 字体: 非加粗, 英语(美国)
设置了格式: 字体: 非加粗, 英语(美国)
设置了格式: 字体: 非加粗, 英语(美国)
设置了格式: 字体: 非加粗, 英语(美国)
设置了格式: 字体: 非加粗, 英语(美国)
设置了格式: 字体: 非加粗, 英语(美国)
设置了格式: 字体: 非加粗, 英语(美国)
设置了格式: 英语(美国)
设置了格式: 字体: 非加粗, 英语(美国)
设置了格式: 字体: 非加粗, 英语(美国)
设置了格式: 字体: 非加粗, 英语(美国)
设置了格式: 字体: 非加粗, 英语(美国)
设置了格式: 字体: 非加粗, 英语(美国)

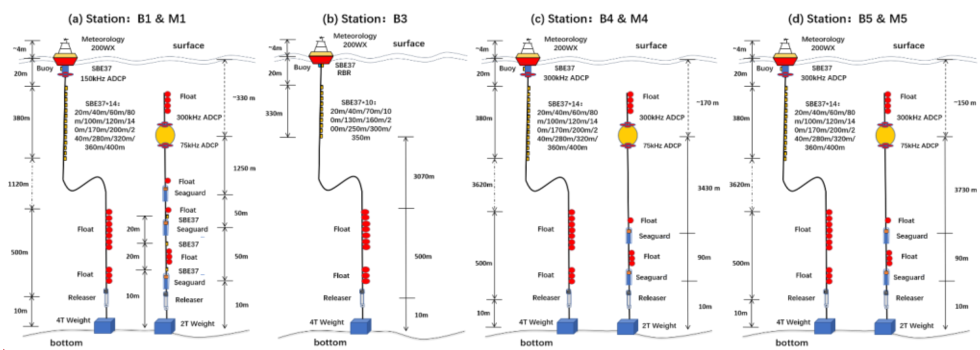

Figure 3~~:~~. Design of stations 1, 3, 4, and 5. Note that all ~~the~~ stations ~~consist of both~~ have a buoy and a mooring, except station 3, which only has a buoy. The dot-and-dash lines indicate the tether length in the middle water of the buoy, ~~while~~ whereas the dashed lines indicate the depth of the two acoustic Doppler current profilers (ADCPs) on the top of the mooring.

Table 2. Observation data details at each station

	Stations	Recorded Data	Equipment and Position	Time Resolution
Buoy Location 1	B1~~-~~–B5	Longitude (°E), Latitude (°N)	GPS sensor 1	1 h
Buoy Location 2			GPS sensor 2	
Buoy Location 3	B1, B2, B4, B5		GPS sensor 3	1 h (B1, B4), 3 h (B2) or 6 h (B5)
Meteorological data 1	B1~~-~~–B5	Air temperature (°C), Air pressure (hPa), Relative humidity (%), Compass (°), Wind speed (m/s, average and maximum), Wind direction (°, average and maximum), Rain guage (mm), Compass (°)	Meteorological sensors at 4 m height from sea surface	12 min (B2) or 1 h (B1, B3, B4, B5)
Meteorological data 2			Auto meteorological station (200WX) at 4 m height from sea surface	
Current 1*	B1, B2, B4, B5, M1, M2, M4, M5	Speed (cm/s), Direction (°), Vertical velocity (cm/s), Temperature, Bin (m), Real-time and designed depth of the ADCP (m, ~~Depth~~ depth and ~~Depth 0~~ depth0)	Downward~~-~~-looking for ADCP 1, 3, and uplooking for ADCP 2	3 min (300 and 150 kHz ADCP) or 15 min (75 kHz ADCP)
Current 2	M1, M2, M4, M5	Speed (cm/s), Direction (°)	SeaGuard at 10 ~~m~~ (M1, M2, M4, M5), 50 ~~m~~ (M1) and 100 m (M1, M2, M4, M5) from ocean bottom	10 min

设置了格式: 英语(美国)
设置了格式: 英语(美国)
设置了格式: 英语(美国)
设置了格式: 字体: 非加粗, 英语(美国)
设置了格式: 字体: 非加粗, 英语(美国)
设置了格式: 字体: 非加粗, 英语(美国)
设置了格式: 字体: 非加粗, 英语(美国)
设置了格式: 字体: 非加粗, 英语(美国)
设置了格式: 字体: 非加粗, 英语(美国)
设置了格式: 字体: 非加粗, 英语(美国)
设置了格式: 字体: 非加粗, 英语(美国)
设置了格式: 英语(美国)

Sea temperature, salinity and pressure	B1, B2, B4, B5, M1	Temperature (°C), Salinity (psu), Pressure (dbar), Depth (m)	SBE-37 with design depth (m) at buoys: 20, 40, 60, 80, 100, 120, 140, 170, 200, 240, 280, 320, 360, 400~~.~~ SBE-37 with design depth 10 ~~m~~ and 50 m above the bottom at M1	2 min
Sea Surface Waves	B1, B4	Wave height (m, Significant and Maximum), Peak period (s), Mean wave direction (°), Wave spread	Wave gauge at sea surface (0 m)	1 h
Radiation (W/m^2)	B3	Short wave (upward, downward), Long wave (upward, downward), Air temperature (°C)	Wave radiometer at 4 m height from sea surface	1 h
Visibility (VIS, km)		Air visibility (km)	Visibility meter at 4 m height from sea surface	
Biochemistry data		Water pressure (dbar), Turbidity (V, two sensors), Chlorophyll (ug/L, Chla), Colored dissolved organic matter (ppb, CDOM)	RBR sensors at sea surface (0 m)	12 min

* Acoustic Doppler current profiler (ADCP) 1 was the downward~~-~~ looking ADCP deployed at the buoy, ~~ADCP~~ADCPs 2 and 3 were the upward and downward~~-~~ looking ADCPs on the mooring~~.~~, respectively. The 300 kHz ADCPs were binned in 4 m, with the first bin at 8 m (B4) or 6.24 m (M1, M2) and the last bin at 124 m (B4) or 122.24 m (M1, M2). The 150 kHz ADCPs were binned in 8 m, with the first bin at 14 m and the last bin at 246 m. ~~75kHz ADCP~~The 75 kHz ADCPs were binned in 16 m intervals, with the first bin at 24.7 m and the last bin at 568.7 m. ADCP 1 at B5 was lost during observation and no data were recovered.

2.2 Dataset description

The dataset ~~is composed of~~comprises 52 files in netcdf file (.nc) format containing air and ocean observation data ~~as well as~~and the positions of the buoys during ~~the period of~~ 2014–2015, along with a metadata file in~~-~~ .txt format to ~~give a brief introduction of~~briefly introduce the data. The observation instruments were calibrated before deployment ~~and the~~. After output from the observation instruments, the observation data are transformed directly to netcdf files ~~after output from the observation instruments,~~, with the units and FillValues labeled. No special modification or ~~say~~ quality control was applied ~~in order~~ to keep the original output data unchanged. All the files include ~~time values both~~ Coordinated Universal Time (UTC) and local time, which is eight hours ahead of ~~the Coordinated Universal Time~~UTC (UTC +8) since 0000-01-01 00:00:00. The local time is also called China Standard Time ~~(CST)~~ or Beijing Time ~~(BJT).~~. The location data ~~includes~~are longitude (°E) and latitude (°N~~)~~), observed by Global Positioning System (GPS) sensors. ~~There were~~ B1, B2, B4, and B5 had three GPS sensors ~~on buoys 1, 2, 4, and 5~~, and B3 had two ~~GPS sensors on buoy 3.~~. Location-1 data ~~was~~were obtained from the ~~main~~primary GPS sensors on the body of the buoys, Location-2 data ~~was~~were obtained from the GPS sensors approximately 4 m above the sea surface, and Location-3 data ~~was~~were obtained from the low-frequency GPS sensors at the bottom of the buoys (approximately 0 m). The measurement accuracies of the GPSs were <50 m.

设置了格式: 英语(美国)
设置了格式: 英语(美国)
设置了格式: 英语(美国)
设置了格式: 英语(美国)
设置了格式: 英语(美国)
设置了格式: 英语(美国)
设置了格式: 英语(美国)
设置了格式: 英语(美国)
设置了格式: 英语(美国)
设置了格式: 英语(美国)
设置了格式: 英语(美国)
设置了格式: 英语(美国)
设置了格式: 英语(美国)
设置了格式: 英语(美国)
设置了格式: 英语(美国)

The air data includesinclude observations approximately 4 m above the sea surface from meteorological sensors (Meteorologymeteorology data) and the automatic meteorological station (200WX data). In Two sets of meteorological stations are deployed on the buoys in order to haveprovide a backup in case whenif the sensors of a meteorological station break down during observation. The 200WX data are similar to the meteorology data, but does not includeexclude rain guagegauge data. The wind direction of wind indicates the direction of the incoming wind; for example, 0° indicates wind passing from north to south, and 90° indicates wind passing from east to west. The compass indicates the direction of the compass on the meteorological sensors or stations, which refersreferring to the attitude of the sensors or stations. For the measurement accuracies of 200WX, the air pressure is ±1 hPa, the air temperature accuracy is ±1.1 °C, the relative humidity is ±5 %, the compass is 1° for static heading and 2° for dynamic heading, whileand the measurement accuracy of wind is differentdiffers in dry and wet conditions. In dry conditionconditions, the wind speed accuracy is 0.5 m/s + 10% of reading for low winds (0 to 5 m/s), or thea greater value of 1 m/s or 10% for high winds (5 to 40 m/s), the wind direction accuracy is 5° for low winds (2 to 5 m/s) and 2° for high winds (>(≥5 m/s). In wet conditionconditions, the wind speed accuracy is 2.5 m/s and 8°. The measurement accuracy of the meteorological sensors hasis in the same order withas 200WX. For the meteorology data of buoy 3B3, there was a visibility meter to measure air visibility (km), while also a Campbell Scientific NR01 four-component net radiometer approximately 4 m above the sea surface with outputs every 1 h, measured upward and downward shortwave and longwave radiation (W/m^2) as well as), and air temperature observed by the radiometer (°C). The measurement accuracy is ±10% of the measurement range for air visibility, <≤2.4 % the measurement range% for shortwave radiation, and <≤7 % for longwave radiation.

The ocean data includes sea surface waves observed by a TRIAXYS™ OEM wave recorder (Wave data), the temperature, salinity, and pressure using conductivity, temperature, and depth (CTD) recorders observed by Sea-Bird Scientific 37 recorders (SBE data), currents observed by Teledyne RD Instruments (TRDI) acoustic dopplerDoppler current profilers (ADCP data)), and currents observed by Aanderaa Data Instruments SeaGuard Recording Current Meter (SeaGuard data), andas well as Biochemistry data observed by multi-parameter Richard Brancker Research (RBR) sensors (RBR data). The 75 kHz ADCP was a TRDI Workhorse Long Ranger, the 150 kHz ADCP was a TRDI Workhorse Quartermaster, and the 300 kHz ADCP was a TRDI Workhorse Sentinel. Sea surface wave data includes significant wave height (m), maximum wave height (m), mean wave direction (°), peak period (s), and wave spread (Table 2). The observation accuracy is better than 2% of the measurement range for pressure for wave height and period, while and ±1° for wave direction. Wave recorders were deployed on buoys 1, 4B1, B4, and 5B5, but the wave recorder on buoy 5B5 broke down, resulting in low-quality data. Consequently, only sea surface wave data from buoys 1B1 and 4B4 were included in the ocean data.

SBE data includesinclude temperature (°C), salinity (psu), and pressure (dbar) observed by SBE-37 CTD sensors. The measurement accuracies of SBE-37 isare ±0.002 °C ((−5 to 35 °C) or ±0.01 °C (35 to 45 °C) for temperature, ±0.0003 S/m for electrical conductivity, and 1% of the measurement range for pressure. Serial 1 to 15 in the SBE data refersrefer to the SBE-37 sensors from the surface to the ocean bottom. All SBE sensors are deployed on the buoys, except for three SBE-37s on the moorings ~~located~~ near the ocean bottom (Figs. 1b and 2). ~~Note that the~~ The SBE-37 strings on ~~buoys 1~~B1 and ~~3~~B3 were lost during deployment ~~period, so~~; therefore, only SBE data at the sea surface ~~located~~ at the bottom of the buoy (Temperature1, Salinity1, and Pressure1) ~~was~~were obtained. Two SBEs on ~~buoy 4~~B4 broke down during observation, resulting in data from only 13 SBEs. The ADCP data ~~consists of~~comprise current speed (cm/s ~~Speed~~), current direction (° ~~direction~~), temperature observed by ADCP (°C ~~temperature~~), depth of the ADCP (m ~~depth~~), designed depth (depth0), and bin intervals of the ADCP observation (m ~~bin~~). The SeaGuard data ~~includes~~include current speed (cm/s ~~speed~~) and ~~current~~ direction (° ~~direction~~). Unlike wind direction, current direction indicates the direction of the current flow~~,~~; for example, 0° indicates the current passing from south to north, and 90° indicates the current passing from west to east. In SeaGuard data, the accuracy is ±1° of reading for current speed~~, while~~ and ±3° (if the tilt is 0~~ – ~~15°) or ±5° (if the tilt is 15~~ – ~~35°) for the current direction.

Negative ~~Bin~~bin values refer to downward-looking ADCPs and vice versa. ADCPs on the buoys (ADCP 1) were downward-looking, located at the sea surface (approximately 0 m~~), so~~); their observation range was depth0 + bin. The ADCP data on the moorings ~~consist of~~comprise upward-looking (ADCP 2) and downward-looking (ADCP 3) observations with ranges depth + Bin~~, as~~ because the depth of the ADCPs at the moorings varies during observation. ~~Note that buoy 3~~B3 did not have ADCP or SeaGuard ~~observation (see~~ observations (Fig. 3 and Table 2), and the ADCP at ~~buoy 5~~B5 broke down, and no data were obtained. For the bin sizes of the ADCPs, the 300 kHz ADCPs were binned in 4 m, with the first bin at 8 m (~~buoy 4~~B4) or 6.24 m (~~mooring 1~~M1 and ~~2~~M2) and the last bin at 124 m (~~buoy 4~~B4) or 122.24 m (~~mooring 1~~M1 and ~~2).~~M2). The 150 kHz ADCPs were binned in 8 m, with the first bin at 14 m and the last bin at 246 m. ~~75kHz ADCP~~The 75 kHz ADCPs were binned in 16 m intervals, with the first bin at 24.7 m and the last bin at 568.7 m. The velocity accuracy for the 75 kHz ~~ADCP~~ADCPs is 1% of water velocity relative to the ADCP ±0.01 m/s (written as 1% ~~±~~ ± 0.01 m/s~~), while the~~). The accuracies for the 150 and 300 kHz ~~ADCP~~ADCPs are 1% ~~±~~ ± 0.005 m/s and 0.5% ~~±~~ ± 0.005 m/s, respectively. The RBR sensors were only deployed at ~~buoy 3,~~B3 and observed water pressure (dbar), turbidity (V) by two sensors, chlorophyll (ug/L Chla~~)~~), and ~~Colored~~colored dissolved organic matter (~~ppb~~ CDOM; ppb). The measurement accuracy of water pressure was ±0.05 ~~% of measurement range for water pressure, ±2% of the measurement range~~%, ±2% for turbidity and chlorophyll, and ±0.01 ppb for CDOM~~,~~.

3 Results

The data at station 2 (B2 and M2) were ~~long~~longer and more complete ~~relative to~~than those at the other stations~~,~~ and ~~is~~are shown first to provide an example of the observations at the stations. Subsequently, observations differing from station 2 are also shown, including near-bottom observations at B1, sea surface waves at B1 and B4, and the observations at B3 after its rope snapped on ~~15~~ September 15, causing it to become a drift.

设置了格式: 英语(美国)
设置了格式: 英语(美国)
设置了格式: 英语(美国)
设置了格式: 英语(美国)
设置了格式: 英语(美国)
设置了格式: 英语(美国)
设置了格式: 英语(美国)
设置了格式: 英语(美国)
设置了格式: 英语(美国)
设置了格式: 英语(美国)
设置了格式: 英语(美国)
设置了格式: 英语(美国)

3.1 Sea surface air and ocean observation at station 2

The prevailing wind direction was approximately 200° (nearly south wind) from late July to mid-August, then shifted primarily in the range of 20°–80° (nearly northeast wind) after October, with wind direction variations during September (Fig. 4b, d). This finding indicates that the transition occurred from local summer to winter monsoon, with September as the transition month. ~~Average~~The average wind speed ~~is~~was less than 10 m/s during July and August, often exceeding 10 m/s after October (Fig. 4a, c), indicating that the winter monsoon was stronger than the summer monsoon at B2. B2 likely traveled through the eye of typhoon Kalmaegi, with two ~~peaks in~~ wind speed peaks accompanied by minimum air pressure (Zhang et al., 2016). ~~Note that typhoon~~Typhoon Kalmaegi and severe tropical storm Fung-wong during September significantly influenced the wind direction at B2, with the wind direction turning ~~counter-clockwise~~counterclockwise near September 15 and 21, consistent with B2 being on the left side of both TCs.

B2 also recorded a drop in sea surface air and ocean temperature (Fig. 4g, i) from summer to winter, ranging from approximately 28.5 °C to 30.5 °C in August, decreasing from approximately 29 °C to ~~approximately~~ 27 °C in October, and continuing to decrease further. ~~Surface~~The surface air temperature was slightly lower than the sea surface temperature during the observation period, indicating local sensible heat flux from the ocean to the atmosphere~~, as~~ because the water cooled slower than air during ~~autumn. The~~ fall. Due to their high time resolution (2 min), the observations also captured the diurnal ~~variation of~~ temperature~~,~~ variation attributed to daytime solar radiation heating~~ and~~, nighttime outward longwave radiation cooling, and the deepening of the ocean mixed layer~~, were also captured by the observations due to their high time resolution (2 min).~~. Typhoon Kalmaegi and tropical storm Fung-wong successively decreased the sea surface air and ocean temperatures during September, with Kalmaegi suddenly decreasing the sea surface temperature by approximately 2.5 °C~~, as~~ because B2 was located in the core cooling area on the right-hand side of the typhoon track.

Rain ~~guage~~gauge data ~~was~~were measured ~~by~~using a tipping bucket rain gauge, with a maximum measurement of 255 mm. The bucket empties when full (255 mm~~)~~), and the measurement starts from 0 mm again. ~~Rain~~The rain rate can be calculated by dividing the difference in rain ~~guage~~gauge values by the time interval. Significant rainfall events were recorded ~~near 2~~around August~~, 6~~ 2, September 6, 15~~ September~~, and 21~~ September. The strong rainfall near 15 September and 21 September was induced by typhoon~~. Typhoon Kalmaegi and severe tropical storm Fung-wong~~. Note that evaporation~~ induced strong rainfall around September 15 and 21. Evaporation also affected rain ~~guage~~gauge values, which decreased slowly over time without precipitation, indicating that rain ~~guage~~gauge data reflected precipitation and evaporation. Sea surface salinity increased from approximately 33.3 psu near ~~1~~ October 1 to approximately 33.8 psu near ~~10~~ November 10 (Fig. 4i~~), owing~~) due to little rainfall~~ during this period~~, with salinity primarily controlled by evaporation.

~~There were some consistencies~~Some similarities and differences existed between the two ~~sets of~~ meteorological observations~~,~~: the European Centre for Medium-~~Range~~range Weather Forecasts (ECMWF) Reanalysis v5 data (ERA5, https://www.ecmwf.int/en/forecasts/dataset/ecmwf-reanalysis-v5) ~~is~~are used to evaluate ~~the~~their performance~~ of them~~. The average and maximum wind speed and direction in the ~~Meteorology~~meteorology and 200WX datasets are consistent~~ while~~,

设置了格式: 英语(美国)
设置了格式: 英语(美国)
设置了格式: 英语(美国)
设置了格式: 英语(美国)
设置了格式: 字体: 10 磅, 英语(美国)
设置了格式: 字体: 10 磅, 英语(美国)

and the average wind matched the wind speed from ERA5 well, except that the average wind direction observed by meteorological sensors suddenly turned to approximately 180°, and the maximum wind direction varied rapidly between 0° and 360° after 15 November 15 (Fig. 4b, d), indicateindicating some malfunctions of the wind meteorological observation sensor. Air pressure measurements from the meteorological sensors, 200WX station, and ERA5 are consistent before 27 August 27, with the diurnal variation of air pressure variation observed by the meteorological sensors amplifying and becoming inconsistent with the 200WX observations and ERA5 after 27 August 27 (Fig. 4f), indicateindicating some malfunction of the pressure meteorological observation sensor. The sensitivity of the air temperature measurements by the 200WX was greater than that of the temperature meteorological sensor, with larger amplitude diurnal variations, whilewhereas their values of both of themwere a bit greater or different withfrom ERA5 data (Fig. 4g). Relative humidity measured by the meteorological sensor was consistent with ERA5 data and was greater than that measured by the 200WX, ranging from 0 % to 10 % (Fig. 4h). Both two sets of meteorological observations showed missing data aboutapproximately 5 days near 6 October 6, which maymight be due to the malfunction of the instruments or data recording.

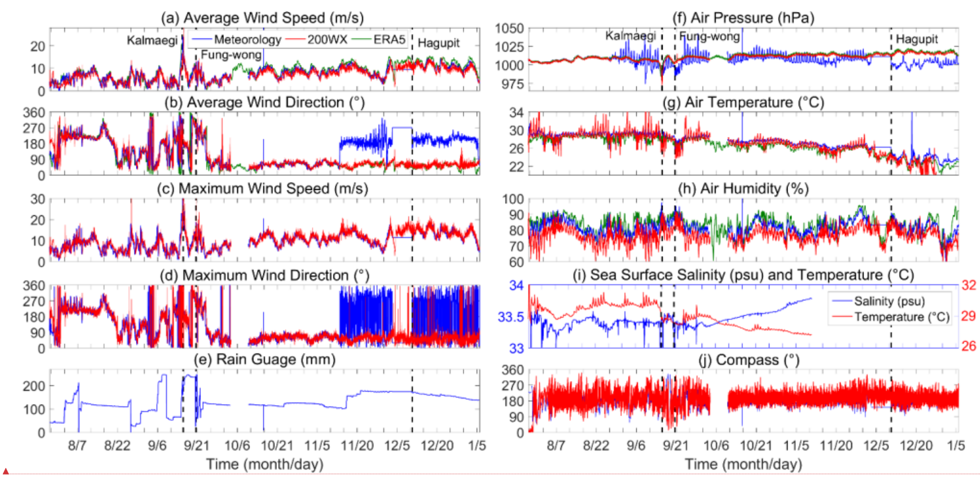

Figure 4: Observation at Buoy 2. **Average** (B2): the average and maximum wind speedspeeds (**a**, **b**; m/s) and direction (**c**, **d**; °), rain guagegauge (**e**; mm), air pressure (**f**; hPa), air temperature (**g**; °C), relative humidity (**h**; %), sea surface salinity (**i**; psu), sea surface temperature (**i**; °C), and buoy compass (**j** °). **Blue**; °). The blue and red lines are data observed by the meteorological sensors and the 200WX automatic meteorological station, approximately 4 m above the sea surface, while. The blue and red lines in (**i**) represent salinity and temperature observed by the SBE-37 sensor at the buoy bottom (approximately 0 m). **Wind**The wind directions indicate the direction from which the wind originates. The vertical dashed lines indicate the time when TCTCs Kalmaegi, Fung-wong, and Hagupit were closest to **Buoy 2**B2. The green lines are the European Centre for Medium-**Range**range Weather Forecasts (ECMWF) Reanalysis v5 (ERA5) data.

设置了格式: 英语(美国)
设置了格式: 英语(美国)
设置了格式: 英语(美国)
设置了格式: 字体: 非加粗
设置了格式: 字体: 非加粗
设置了格式: 字体: 非加粗
设置了格式: 字体: 非加粗
设置了格式: 字体: 非加粗
设置了格式: 字体: 非加粗
设置了格式: 字体: 非加粗
设置了格式: 字体: 非加粗
设置了格式: 字体: 非加粗
设置了格式: 字体: 非加粗
设置了格式: 字体: 非加粗
设置了格式: 字体: 非加粗
设置了格式: 字体: 非加粗
设置了格式: 字体: 非加粗
设置了格式: 字体: 非加粗
设置了格式: 字体: 非加粗
设置了格式: 字体: 非加粗
设置了格式: 字体: 非加粗
设置了格式: 字体: 非加粗
设置了格式: 字体: 非加粗
设置了格式: 字体: 非加粗
设置了格式: 字体: 非加粗
设置了格式: 字体: 非加粗
设置了格式: 字体: 非加粗, 英语(美国)
设置了格式: 字体: 非加粗, 英语(美国)
设置了格式: 字体: 非加粗
设置了格式: 英语(美国)

3.2 Current, temperature, and salinity observation at station 2

设置了格式: 英语(美国)

At station 2, the current observations at the mooring (~~Fig~~Figs. 5b–d) were longer than those at the buoy (Fig. 5a), ~~as well as~~and the temperature and salinity (Fig. 6) observations at the buoy~~,~~ due to the deployment and recovery times. The upward-looking 300 kHz ADCP (Fig. 5b) and the SBE-37 recorder at the bottom of the buoy (Fig. 6) stopped working near ~~11~~ November~~,~~ 11 while the data quality from the downward-looking 75 kHz ADCP at the mooring decreased, especially in ~~year~~ 2015, with some missing data at several bins (Fig. 5b). Although the ~~length of the~~SBE chain ~~of SBEs~~ was 400 m long, the observation range of temperature and salinity was primarily shorter than 400 m~~, as~~ because the rope swung and tilted during ~~observation~~observations, especially the deepest observation depth decreased to ~200 m near ~~21~~ September 21 under the influence of typhoon-induced near-inertial waves after Kalmaegi. Similarly, the positions of the ADCPs at the moorings also moved vertically due to the tilt of the mooring rope, especially when influenced by intensified currents after ~~-~~Rammasun and Matmo in July~~,~~ and Kalmaegi in September.

~~Horizontal~~ADCPs and SeaGuards captured horizontal currents induced by diurnal and semi-diurnal tides ~~were captured by ADCPs and SeaGuards, along with diurnal and semi-diurnal~~as well as vertical variations ~~of~~in temperature and salinity isolines. The upper ocean background current speed was primarily <20 cm/s, significantly increasing after ~~tropical cyclones, e.g.,~~TCs Rammasun and Matmo in July, Kalmaegi in September, and Hagupit in December, with the mixed layer current speed reaching approximately 150 cm/s after Kalmaegi (Zhang et al., 2016). Typhoon Kalmaegi immediately strengthened the near-inertial mixed layer currents and kinetic energy, which then propagated horizontally and vertically with the dispersion of near-inertial waves and regulation by background vorticity (Lu et al., 2023; Lu et al., 2024; Zhang et al., 2016). Near-bottom currents were ~~mainly~~primarily <10 cm/s~~, while~~ and near-bottom flow turned from northeastward to southeastward after the influence of typhoon Rammasun.

~~Upper~~The upper ocean temperature decreased monotonously from the surface (approximately 0 m) to approximately 400 m, and salinity exhibited a "low–high–low" vertical structure with a maximum of approximately 34.5 psu from approximately 100 m to ~~approximately~~ 250 m. There is long-term upper ocean cooling and a decrease in salinity from summer to winter (Fig. 6), especially after mid-October. Kalmaegi reduced the sea surface temperature by approximately 1.9 °C at its maximum, with a subsurface cold anomaly of approximately 1.1 °C ~~at its maximum~~ (Zhang et al., 2016) ~~owing~~due to its proximity to the typhoon track, where ~~upper ocean temperature was primarily modulated by~~ typhoon-induced mixing and upwelling primarily modulated the upper ocean temperature (Zhang, 2023; Zhang et al., 2018). Vertical variations ~~of~~in temperature and salinity were also influenced by~~ processes such as~~ eddies, fronts, and flows (Liu et al., 2017; Lu et al., 2024), but these are not pursued further here. The downward propagation of warm or freshwater anomalies from the surface~~, along with~~ and the diurnal cycle of the near-surface mixed layer~~,~~ can also be observed (Fig. 6) and partly analyzed in Zhang (2023).

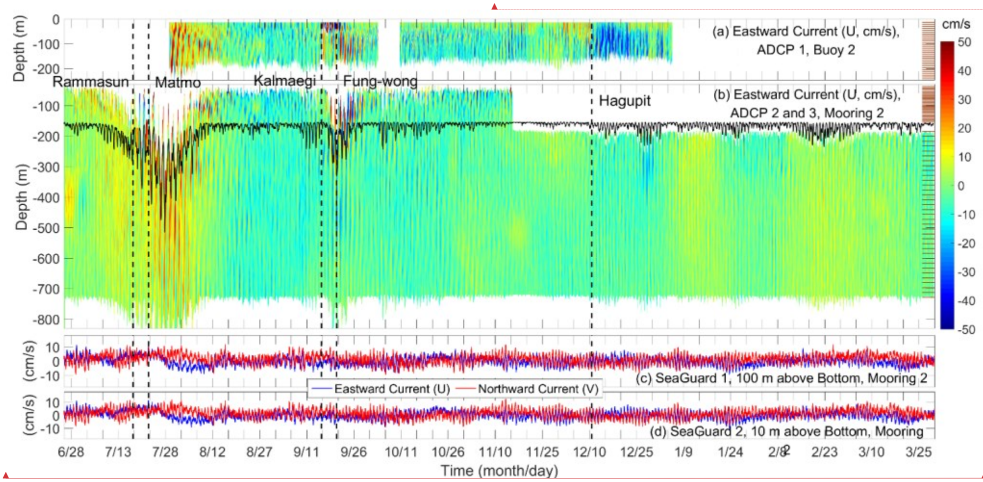

Figure 5~~:~~. **(a–b~~):~~)** Eastward currents (m/s) observed by the downward-looking 150 kHz ADCP at the buoy bottom **(a)~~,~~** and the combination of the upward-looking 300 kHz and downward-looking 75 kHz ~~ADCP~~ADCPs at the mooring **(b)**. **(c~~-~~, d)** Eastward (U) and northward (V) currents are observed by the SeaGuard current meter at 100 m **(c)** and 10 m **(d)** above the ocean bottom. ~~Black~~The black solid line in **(b)** represents the vertical positions of ~~ADCP~~ADCPs 2 and 3. The vertical dashed lines represent the time when ~~tropical cyclones~~the TCs are closest to Buoy 2. The brown lines in **(a)** and **(b)** represent the initial depth of the observation bins of the ADCPs.

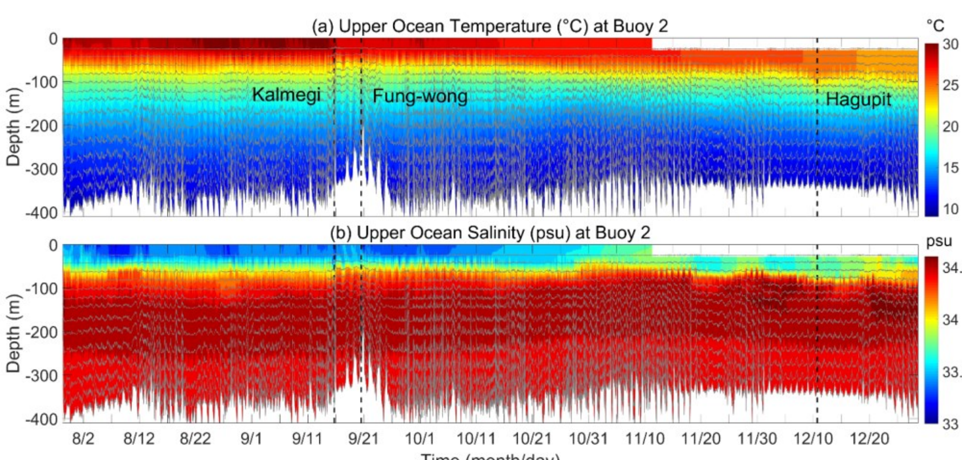

Figure 6~~:~~. Upper ocean temperature (**a**~~:~~, °C) and salinity (**b**~~:~~, psu) observed by the chain of SBE-37 sensors at buoy 2. The vertical dashed lines ~~indiate~~indicate the time when ~~tropical cyclones~~the TCs are closest to Buoy 2. ~~Gray~~The gray lines represent the time variation of the depth of the SBE-37 sensors.

设置了格式
设置了格式: 英语(美国)
设置了格式
设置了格式: 英语(美国)
设置了格式: 英语(美国)
设置了格式

3.3 Near-~~-~~bottom observation at mooring 1

The instruments at M1 differed from those at other moorings~~, so~~; their observations are analyzed and discussed here. Three SBEs were deployed near the ocean bottom ~~in order~~ to ~~check~~evaluate the homogeneity of the near-bottom layer. The variation ~~of~~in near-bottom pressure observed by the three SBEs at approximately 10 ~~m~~, 30 ~~m~~, and 50 m above the ocean bottom is ~~very small~~tiny (Fig. 7a), indicating minimal swing and tilt of the rope near the bottom of M1. The water pressure at approximately 10 m above the bottom was approximately 1710 dbar, corresponding to a depth of approximately 1690 m, indicating that the water depth of M1 was approximately 1700 m. The temperature varied from 2.5 °C to 2.7 °C, and salinity ~~is~~was close to 34.6 psu at the three SBEs (Fig. 7b, c). The temperature, salinity, and currents observed from the three SBEs and SeaGuards were ~~very~~ close, indicating a uniform near-bottom layer greater than 100 m (Fig. 7d). However, the current at 100 m above the bottom differed from the other two layers during ~~29~~ July 19 to ~~12~~ August 12 and ~~20~~ December 13 to ~~13 December~~20, when the near-bottom flow also turned at M1, possibly influenced by super typhoons Rammasun and Hagupit (Fig. 7e).

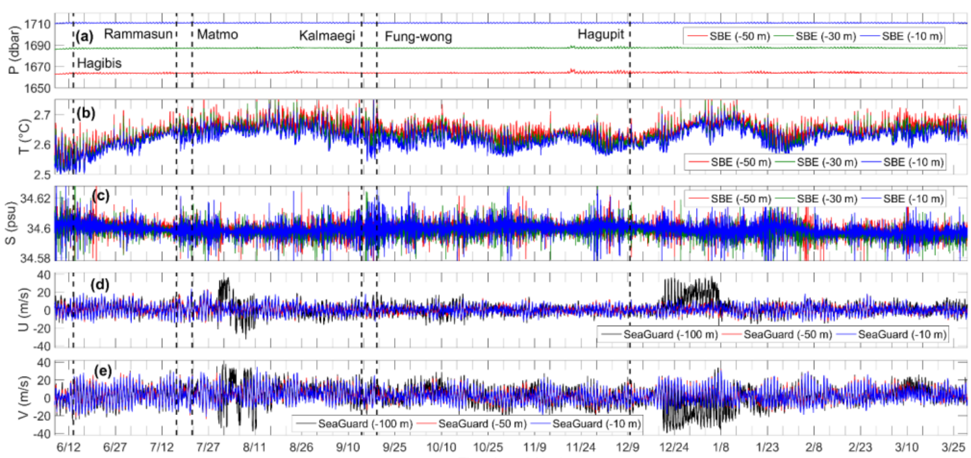

Figure 7~~:~~. **(a–c)**~~:)~~ Pressure (dbar; **a**), temperature (°C; **b**), and salinity (psu; **c**) observed by the SBE-~~37~~37s at the mooring at approximately 50 ~~m~~ (red), 30 ~~m~~ (green), and 10 m (blue) above the ocean bottom. **(d–e)** Eastward current (cm/s) and northward current observed by the SeaGuard current meter at the mooring at approximately 100 ~~m~~ (black), 50 ~~m~~ (red), and 10 m (blue) above the ocean bottom. The vertical dashed lines represent the time when ~~**tropical cyclones**~~the TCs were the closest to Mooring 1.

3.4 Sea surface waves

Sea surface waves observed at B1 and B4 also merit further explanation. The variations ~~of~~in sea surface waves from the two wave gauges at B1 and B4 are similar (Fig. 8), indicating that the ~~characteristic~~characteristics of the sea surface waves at the observation array were comparable. However, B4 showed more drastic variation ~~of~~in the peak period than B1, with

设置了格式: 英语(美国)
设置了格式: 英语(美国)
设置了格式: 英语(美国)
设置了格式: 英语(美国)
设置了格式: 英语(美国)
设置了格式: 字体: 非加粗, 英语(美国)
设置了格式: 字体: 非加粗, 英语(美国)
设置了格式: 英语(美国)
设置了格式: 字体: 非加粗, 英语(美国)
设置了格式: 字体: 非加粗, 英语(美国)
设置了格式: 英语(美国)
设置了格式: 字体: 非加粗, 英语(美国)
设置了格式: 字体: 非加粗, 英语(美国)
设置了格式: 英语(美国)
设置了格式: 字体: 非加粗, 英语(美国)
设置了格式: 字体: 非加粗, 英语(美国)
设置了格式: 字体: 非加粗, 英语(美国)
设置了格式: 字体: 非加粗, 英语(美国)
设置了格式: 英语(美国)
设置了格式: 英语(美国)
设置了格式: 字体: 非加粗, 英语(美国)
设置了格式: 字体: 非加粗, 英语(美国)
设置了格式: 字体: 非加粗, 英语(美国)
设置了格式: 字体: 非加粗, 英语(美国)
设置了格式: 英语(美国)
设置了格式: 英语(美国)

different mean wave ~~direction~~directions and wave ~~spread during~~ spreads from July 14 to 20 ~~July~~ and near ~~26~~ July~~, which may due to~~ 26, indicating the influence of ~~tropical cyclones~~TCs Habibis and Matmo. The ~~observation~~observations at B1 were longer than at B4~~,~~ but with some ~~miss recording near 1~~ missing recordings from August 1 to ~~17~~ August~~.~~ 17.

Sea surface ~~waves were mainly controlled by sea surface~~ winds, e.g., monsoon and ~~tropical cyclones.~~TCs, primarily controlled the sea surface waves. During the summer monsoon (before September), the significant wave height was primarily <2 m, maximum wave height <3 m, peak period <10 s, and the mean wave direction was close to 180° (northward). During the winter monsoon (after October), significant and maximum wave heights increased to >3 m and >5 m, respectively, ~~as well as~~and the peak period ~~>~~ to >10 s and the mean wave direction nearly 90° (westward). ~~Wave~~The wave spread ranged from 20 to 80 throughout the observation period of the two wave gauges (Fig. 8e).~~Tropical cyclones~~ The TCs strongly influenced the local sea surface waves. Significant wave height increased to approximately 5~~ m~~, 10~~ m~~, and 3 m (Fig. 8a), ~~while~~whereas maximum wave height reached approximately 8~~ m~~, 15–18~~ m~~, and 5–6 m (Fig. 8b) ~~due~~owing to the influence of ~~tropical cyclones~~TCs Rammasun, Kalmaegi, and Fung-wong, respectively. ~~Sea~~The sea surface wave height increased rapidly in one day, along with a clockwise rotation of the mean wave direction and an increase in the peak period, then returned to background conditions within approximately three days, with the mean wave direction rotating counterclockwise and a decrease in the peak period (Fig. 8).

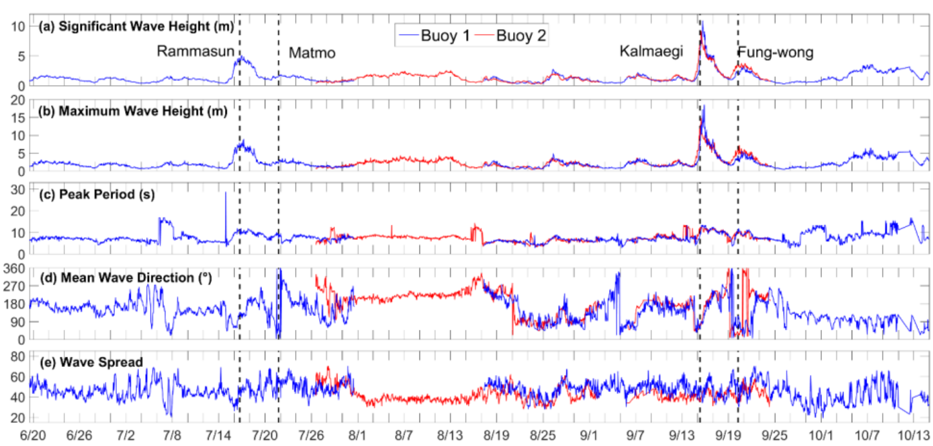

Figure 8~~:~~. Significant wave height (**a**~~;~~, m), maximum wave height (**b**~~;~~, m), peak period (**c**~~;~~, s), mean wave direction (**d**~~;~~, °), and wave spread observed by the wave recorders at the bottom of buoys 1 (blue) and 4 (red). The vertical dashed lines represent the time when ~~**tropical cyclones**~~the TCs were the closest to the moored array.

设置了格式: 英语(美国)
设置了格式: 英语(美国)
设置了格式: 字体: 非加粗, 英语(美国)
设置了格式: 英语(美国)
设置了格式: 字体: 非加粗, 英语(美国)
设置了格式: 英语(美国)
设置了格式: 字体: 非加粗, 英语(美国)
设置了格式: 英语(美国)
设置了格式: 字体: 非加粗, 英语(美国)
设置了格式: 英语(美国)
设置了格式: 字体: 非加粗, 英语(美国)
设置了格式: 字体: 非加粗, 英语(美国)
设置了格式: 英语(美国)

3.5 Observation at buoy 3

~~As~~Since the tether of B3 snapped on ~~15~~ September 15, causing the buoy to ~~became~~become adrift (Fig. 2), it is ~~important~~crucial to describe B3 observations in this section, which partly reflects the air~~-~~–sea conditions in region B3 (Figs. 9 and 10).

The average and maximum wind speeds increased to approximately 20 ~~m/s~~ and 25 m/s, respectively, during Kalmaegi, with the wind direction changing rapidly (Fig. 9a). The average and maximum wind speeds reached approximately 10 m/s during Fung-wong, with the wind direction rotating counterclockwise~~, as~~ because B3 was on the left side of the TC track (Fig. 9b). In October, the wind direction was primarily close to 0°, consistent with B2 (Fig. 4), indicating that the monsoon controlled the local region ~~was controlled by the monsoon~~ from nearly north to south. ~~Rainfall~~The rainfall was strong during Kalmaegi (approximately 250 mm) and Fung-wong (approximately 200 mm), accompanied by low air pressure (980 ~~hPa~~ and 1000 hPa~~), while~~). However, there was little rainfall, and the air pressure increased to more than 1100 hPa after ~~24~~ September ~~(Fig~~24 (Figs. 9e, f). The diurnal ~~variation of~~ air pressure variation can also be found in the observation. ~~Sea~~The sea surface temperature continuously ~~reduced~~decreased from ~30 °C to ~27.5 °C and ~26.5 °C after Kalmaegi and Fung-wong, respectively, and then recovered back to ~29 °C in October (Fig. 10d). Note that the surface air temperature (Fig. 9g) was 1~~-~~–3 °C colder than the sea surface temperature (Fig. 10d) during the observation, ~~indicate that there was~~indicating sensible heat flux from the ocean to the air in Autumn along the track of B3. ~~Relative~~The relative humidity was 85% to 100% during ~~the influence of~~ Kalmaegi and Fung-wong (~~14 to 25~~ September~~),~~ 14–25) and then continuously decreased to approximately 70% in October (Fig. 9h), consistent with the fact that the TC-induced cold wake results in reduced rainfall and sea surface humidity (~~e.g.,~~ Ma et al., 2020). Air visibility was approximately 10 km when B3 was deployed, then decreased to approximately 1 m due to cloud cover and adverse sea surface conditions from typhoon Kalmaegi, and rapidly increased to approximately 16 km on ~~15~~ September 15 due to the passage of the typhoon eye (Fig. 9i). Clear sky returned near ~~17~~ September~~,~~ 17 while subsequent tropical cyclone Fung-wong increased air visibility at B3 to approximately 16 km again on ~~20~~ September 20, lasting until ~~22–23~~ September 22–23.

B3 was the only buoy equipped with a radiometer. The maximum shortwave radiation observed by the upward sensor was approximately 1900 W/m^2 near noon (Fig. 10a~~),~~) when solar radiation was the strongest, significantly reduced by cloud cover from ~~tropical cyclones~~the TCs from ~~13 to 23~~ September~~,~~ 13 to 23 and moderately reduced by local cloud cover in October. Conversely, the shortwave radiation observed by the downward sensor was much (one order) smaller than the upward shortwave radiation, indicating a minimal reflection of solar radiation. Similarly, the longwave radiation observed by the upward and downward sensors was close to 0 W/m^2 and approximately ~~-~~−50 W/m^2 (Fig. 10b), respectively, indicating that longwave radiation was primarily from the ocean to the atmosphere, with minimal contribution from the atmosphere to the ocean. The sea surface temperature (Fig. 10(d)) decreased from approximately 30 °C to ~~approximately~~ 27 °C after Kalmaegi, recovering to approximately 29 °C in October. The air temperature observed by the radiometer (Fig. 10c) followed a similar variation pattern ~~with air temperature~~to that observed by the meteorological sensors (Fig. 9a) and sea surface temperature (Fig.

设置了格式: 英语(美国)

10d), with significant diurnal variation. ~~It is noteworthy that~~The sea surface salinity (Fig. 10d) increased from approximately 33.5 psu to ~~approximately~~ 33.7 psu due to typhoon Kalmaegi, despite strong rainfall (Fig. 9e). The variation in sea surface salinity was consistent with the rain ~~guage~~gauge data, except for a decrease ~~in salinity~~ from ~~3 to 5~~ October~~. There were some~~ 3 to 5.

Some recording errors of sea surface temperature and salinity occurred after ~~5~~ October 5 (Fig. 10d, e~~)~~), with a sudden change ~~of~~in the values. The SBE and RBR sensors were deployed at ~~approximately~~ 1.3 ~~to~~ –1.6 m from the surface, with pressures ~~nearly~~of 1.3 hPa~~–~~–1.6 hPa (Fig. 10f). Chlorophyll observed by the RBR sensor (Fig. 10g) showed diurnal variation, increasing from ~~approximately2 ug/L to~~ approximately 2 ug/L to 2.5 ug/L after Kalmaegi and Fung-wong, then returning to approximately 2 ug/L ~~afterward~~. Turbidity observed by the first sensor (Fig. 10h) is more than 0.05 V before September 15~~,~~. It then decreased to approximately 0.005 V, making it ~~difficult~~challenging to determine whether the decrease ~~is~~was attributable to Kalmaegi, which made the sea surface cleaner, or to damage to the turbidity sensor after ~~B3's~~B3's rope snapped. Conversely, turbidity observed by the second sensor (Fig. 10i) remained near 4.4569 throughout the observation period of B3 (Fig. 10i). ~~Chromophoric dissolved organic matter (~~CDOM~~,~~ (Fig. 10j) gradually increased from 1.88 ppb in September to 2.1 ppb by mid-October.

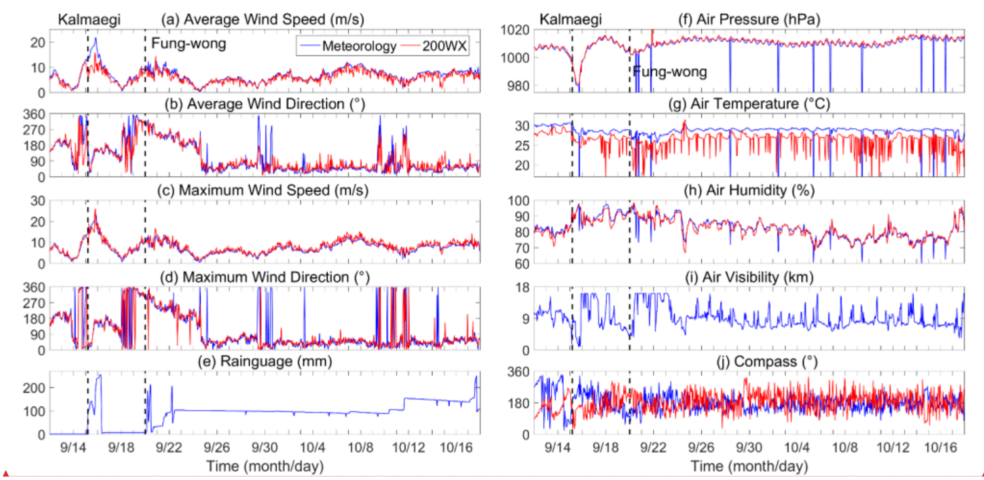

Figure 9~~:~~. Similar to Figure 4 but for buoy 4. ~~**Note that**~~Notably, **(i)** is the air visibility (km) observed by a visibility meter ~~**located**~~ 4 m above the sea surface. The vertical dashed lines represent the time when ~~**tropical cyclones**~~the TCs were the closest to the moored array.

设置了格式: 英语(美国)
设置了格式: 英语(美国)
设置了格式: 英语(美国)
设置了格式: 字体: 非加粗, 英语(美国)
设置了格式: 字体: 非加粗, 英语(美国)
设置了格式: 英语(美国)
设置了格式: 字体: 非加粗, 英语(美国)
设置了格式: 字体: 非加粗, 英语(美国)
设置了格式: 字体: 非加粗, 英语(美国)
设置了格式: 字体: 非加粗, 英语(美国)
设置了格式: 英语(美国)

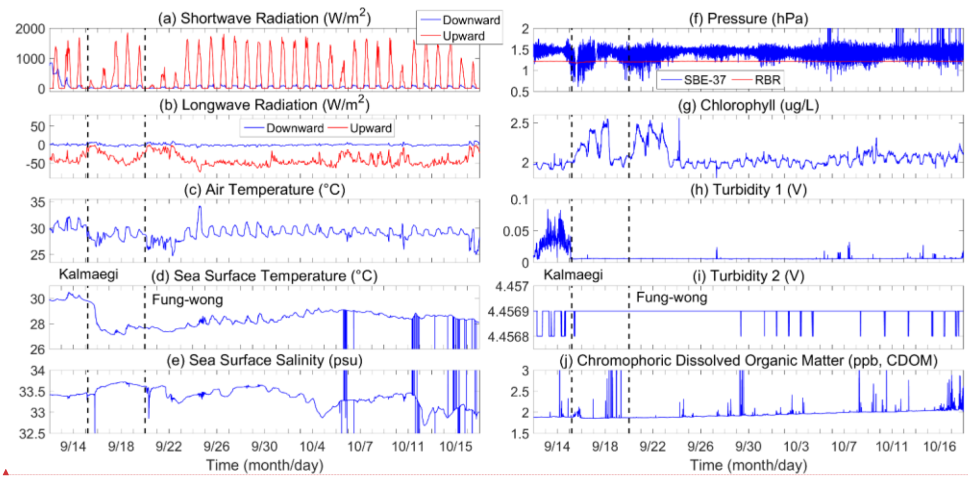

Figure 10~~:~~. Observation at Buoy 3. (a–c~~):~~) Shortwave radiation (a~~,~~; W/m^2) and longwave radiation (b~~,~~; W/m^2) observed by upward (red) and downward (blue) radiation sensors and the air temperature observed by the radiometer (c~~,~~; °C~~) observed by the radiometer.~~). (d–f~~):~~) Sea surface temperature (f~~,~~; °C), salinity (g~~,~~; psu), and pressure (h~~,~~; hPa, blue) observed by SBE-37, with pressure (h~~,~~; hPa~~,~~; red) observed by RBR sensors. (g–j~~):~~) Chlorophyll (g~~,~~; ug/L), turbidity observed by two sensors (g–h~~,~~; V), and chromophoric dissolved organic matter (DCOM; j~~,~~; ppb~~, CDOM). Radiometer~~). The radiometer is ~~located~~ 4 m above the sea surface, ~~while~~and the SBE-37 and RBR sensors are at the bottom of buoy 3 (approximately 0 m). The vertical dashed lines represent the time when ~~tropical cyclones~~the TCs were the closest to the moored array.

4. Data availability

All data are ~~made~~ publicly available through the Zenodo repository ~~with the address:~~at ~~https://zenodo.org/records/13827819~~https://zenodo.org/records/13925651 (Zhang et al~~.~~., 2024). The data will also be publicly available ~~at~~on the website of the Southern Marine Science and Engineering Guangdong Laboratory (Zhuhai) (http://www.hellosea.org.cn/#/metadataDetail/en-US?detailId=8f32902492b84dc1a80f0f717a7c827e) ~~if~~when the manuscript is published. This study provides a detailed dataset description~~ of the dataset, which includes~~, including a time series of sea surface meteorological elements, sea surface waves, ocean temperature, salinity, and currents collected from a moored array ~~consisting of~~comprising five buoys and four moorings during 2014–2015. ~~Meteorological~~The meteorological elements ~~included~~include wind, temperature, pressure, rain ~~guage~~gauge, and humidity data. ~~In addition~~Furthermore, data from the buoy at the center (B3) ~~included~~include sea surface visibility, radiation (shortwave and longwave), and biochemistry observations (chlorophyll, turbidity, and ~~colored dissolved organic matter~~CDOM).

5 Conclusions

This study presents an observation dataset from a cross-shaped moored array ~~consisting of~~comprising five buoys (B1~~-~~–B5) and four moorings (M1, M2, M4, M5) with synchronous atmospheric and oceanic data in the northern ~~South China Sea~~SCS during 2014–2015 (MASCS 1.0). The ~~dataset includes measurements of sea surface~~ atmospheric data are observed by two meteorological ~~data using two sets of~~ instruments~~, sea surface~~ at the buoys. The atmospheric data are observed by two meteorological instruments at the buoys. The oceanic data consist of sea surface waves recorded by a wave recorder~~,~~, and temperature and salinity from the surface to a depth of 400 m~~,~~ and at 10 ~~m~~ and 50 m above the ocean bottom using ~~conductivity, temperature, and depth (~~CTD~~)~~ recorders. It also includes currents from the surface to a depth of 850 m measured by ~~acoustic Doppler current profilers (~~ADCPs~~)~~ and at 10~~ m~~, 50~~ m~~, and 100 m above the floor measured by current meters. Additional measurements were taken for sea surface radiation, air visibility, chlorophyll, turbidity, and ~~chromophoric dissolved organic matter~~CDOM at ~~Buoy 3~~B3, which was ~~located~~ at the center of the moored array. The whole moored array ~~started to be~~was deployed ~~at~~in June 2014 ~~while~~and totally recovered at the end of 2015. Although some instruments ~~as well as~~and buoys broke down or were lost during observation, resulting in no data recovery or ~~data~~ deficiencies, this dataset is valuable for further studies to uncover air~~-~~–sea interactions and oceanic processes in the northern ~~South China Sea~~SCS.

For example, ~~tropical cyclones~~TCs Hagibis in June, Rammasun and Matmo in July, Kalmaegi and Fung-wong in September, and Hagupit in December 2014 traveled over the ~~South China Sea~~SCS and influenced the time series of the observations. The ~~tropical cyclones~~TCs increased the sea surface wind speed, enhanced the sea surface wave height and near-surface ocean currents, cooled the sea surface water and air temperature, also induced near-inertial waves ~~as well as~~and near-bottom currents. The moored array also ~~experienced a transition~~transitioned from the summer to winter monsoons, with prevailing nearly south wind (approximately 200°) and ~~wave~~waves (approximately 180°) with a sea surface significant wave height of <2 m and a peak period of <10 s from late July to mid-August~~,~~. It then shifted to a nearly northeast wind (approximately 20~~°~~ ~~–~~°–80°) and east ~~wave~~waves (approximately 90°~~)~~), with a sea surface significant wave height of >3 m and a peak period of <10 s after October. ~~In addition~~Furthermore, ocean data ~~may~~might have recorded multiscale air~~-~~–sea interactions and ocean processes, such as air~~-~~–sea heat and momentum fluxes, ocean tides, internal waves, seasonal variations in temperature, salinity, and flows, ~~as well as~~and background processes, such as mesoscale eddies and local circulations.

The data ~~has already~~have been used for ~~the analysis of~~analyzing the air~~-~~–sea and ocean variations on the moored array (Quan et al., 2022; He et al., 2024), ~~validation of~~validating ocean (Zhang et al., 2016; Liu et al., 2020; Lu et al., 2023) and air~~-~~–sea coupled (Wu et al., 2020; Lim Kam Sian et al., 2020; Liu et al., 2024) model simulation, ~~check~~evaluating the parameterization of air~~-~~–sea surface flux (Zhang et al., 2020; Liu et al., 2024), ~~investigate~~and investigating the mechanisms and theory of ocean response to ~~tropical cyclones~~TCs (Hong et al., 2022; Zhang 2023). The dataset has the potential for further studies in these fields~~, while may also~~ and can be used for other fields, such as data reanalysis and assimilations.

设置了格式: 英语(美国)

设置了格式: 英语(美国)

Author Contributions. The dataset is made and the whole manuscript is written by HZ, the whole observation project is designed by DC, the flow of the manuscript is revised by TL and DT, the dataset is optimized by MH, QL, and JL.

设置了格式: 英语(美国)

Competing Interests. The contact author has declared that none of the authors has any competing interests.

Financial support. This work has been supported by the National Key R&D Program of China (2023YFF0805300), the Key R&D Program of Zhejiang Province (2024C03257), the Scientific Research Fund of the Second Institute of Oceanography, MNR (JG2309, QNYC2401), the Project supported by Innovation Group Project of Southern Marine Science and Engineering Guangdong Laboratory (Zhuhai) (316323005), the National Natural Science Foundation of China (42227901, 42176015, 42106008), the National Basic Research Program of China (2013CB430300), the Project supported by Southern Marine Science and Engineering Guangdong Laboratory (Zhuhai) (SML2021SP207, SML2021SP102, SML2022SP401), the MEL Visiting Fellowship (MELRS2303), the Zhejiang Provincial Natural Science Foundation of China (LY24D060003), and the Global Change and Air-Sea Interaction II Program (GASI-01-WPAC-STspr), the Open Project of Fujian Provincial Meteorological Administration (2022K02), and the Zhejiang Provincial Natural Science Foundation of China (2022J011078). This research is also supported by the Key Laboratory of Polar Atmosphere-ocean-ice System for Weather and Climate, Ministry of Education, as well as the CMA-FDU Joint Laboratory of Maine Meteorology.

References

Alford, M. H., Peacock, T., MacKinnon, J. A., Nash, J. D., Buijsman, M. C., Centurioni, L. R., Chao, S. Y., Chang, M. H., Farmer, D. M., Fringer, O. B., Fu, K. H., Gallacher, P. C., Graber, H. C., Helfrich, K. R., Jachec, S. M., Jackson, C. R., Klymak, J. M., Ko, D. S., Jan, S., Johnston, T. M., Legg, S., Lee, I. H., Lien, R. C., Mercier, M. J., Moum, J. N., Musgrave, R., Park, J. H., Pickering, A. I., Pinkel, R., Rainville, L., Ramp, S. R., Rudnick, D. L., Sarkar, S., Scotti, A., Simmons, H. L., St Laurent, L. C., Venayagamoorthy, S. K., Wang, Y. H., Wang, J., Yang, Y. J., Paluszkiewicz, T., and Tang, T. Y.: The formation and fate of internal waves in the South China Sea, Nature, 521, 65–69, doi:10.1038/nature14399, 2015.

Cai, Z., Gan, J., Liu, Z., Hui, C. R., and Li, J.: Progress on the formation dynamics of the layered circulation in the South China Sea, Prog. Oceanogr, 181, 102246, doi:10.1016/j.pocean.2019.102246, 2020.

Chen, W., Hu, P., and Huangfu, J.: Multi-scale climate variations and mechanisms of the onset and withdrawal of the South China Sea summer monsoon, Sci. China Earth Sci., 65, 1030–1046, doi:10.1007/s11430-021-9902-5, 2022.

Chen, W., Zhang, R., Wu, R., Wen, Z., Zhou, L., Wang, L., Hu, P., Ma, T., Piao, J., Song, L., Wang, Z., Li, J., Gong, H., Huangfu, J., and Liu, Y.: Recent Advances in Understanding Multi-scale Climate Variability of the Asian Monsoon, Adv. Atmos. Sci., 40, 1–28, doi:10.1007/s00376-023-2266-8, 2023.

Guan, S., Jin, F. F., Tian, J., Lin, II, Pun, I. F., Zhao, W., Huthnance, J., Xu, Z., Cai, W., Jing, Z., Zhou, L., Liu, P., Zhang, Y., Zhang, Z., Zhou, C., Yang, Q., Huang, X., Hou, Y., and Song, J.: Ocean internal tides suppress tropical cyclones in the South China Sea, Nat. Commun., 15, 3903, doi:10.1038/s41467-024-48003-y, 2024.

He, Y., Lin, X., Han, G., Liu, Y., and Zhang, H.: The different dynamic influences of Typhoon Kalmaegi on two pre-existing anticyclonic ocean eddies, Ocean Sci., 20, 621–637, doi:10.5194/os-20-621-2024, 2024.

Hong, W., Zhou, L., Xie, X., Zhang, H., and Liang, C.: Modified parameterization for near-inertial waves, Acta Oceanol. Sin., 41, 41-53, doi:10.1007/s13131-022-2012-6, 2022.

设置了格式: 英语(美国)

Jilan, S.: Overview of the South China Sea circulation and its influence on the coastal physical oceanography outside the Pearl River Estuary, Cont. Shelf Res., 24, 1745–1760, doi:10.1016/j.csr.2004.06.005, 2004.

Li, J., Zhou, C., Li, M., Zheng, Q., Li, M., and Xie, L.: A case study of continental shelf waves in the northwestern South China Sea induced by winter storms in 2021, Acta Oceanol. Sin., 43, 59–69, doi:10.1007/s13131-023-2150-5, 2024.

Lim Kam Sian, K. T. C., Dong, C., Liu, H., Wu, R., and Zhang, H.: Effects of Model Coupling on Typhoon Kalmaegi (2014) Simulation in the South China Sea, Atmosphere, 11, 432, doi:10.3390/atmos11040432, 2020.

Lin, J., Fang, S., Xu, W., Ni, S., Zhang, H., and Yang, T.: Multi-instrument observations of microseisms generated by typhoon Kalmaegi (2014) over the Northwestern Pacific, Earth Planet. Sci. Lett., 594, 117746, doi:10.1016/j.epsl.2022.117746, 2022.

Liu, L., Wang, G., Zhang, Z., and Wang, H.: Effects of drag coefficients on surface heat flux during Typhoon Kalmaegi (2014), Adv. Atmos. Sci., 39, 1501-1518, doi:10.1007/s00376-022-1285-1, 2022.Liu, F., Zhang, H., Ming, J., Zheng, J., Tian, D., and Chen, D.: Importance of Precipitation on the Upper Ocean Salinity Response to Typhoon Kalmaegi (2014), Water, 12, 614, doi:10.3390/w12020614, 2020.

设置了格式: 英语(美国)

Liu, F., Toumi, R., Zhang, H., Chen, D.: Impact of Precipitation on Ocean Responses during Tropical Cyclone. J. Phys. Oceanogr., 54, 895–909, doi:10.1175/jpo-d-23-0138.1, 2024.

Liu, Q., Kaneko, A., and Jilan, S.: Recent Progress in Studies of the South China Sea Circulation, J. Oceanogr., 64, 753–762, doi:10.1007/s10872-008-0063-8, 2008.

设置了格式: 英语(美国)

Liu, S.-S., SUN, L., Wu, Q., and Yang, Y.-J.: The responses of cyclonic and anti-cyclonic eddies to typhoon forcing: the vertical temperature-salinity structure changes associated with the horizontal convergence/divergence, J. Geophys. Res. Oceans, 122, 4974–4989, doi:10.1002/2017JC012814, 2017.

Lu, X., Dong, C., Xu, Z., Yang, J., Zhang, H., Wang, D., and Chen, D.: Effects of numerical model's horizontal resolution on the vertical transport of near-inertial energy, Deep-Sea Res. II, 207, 105223, doi:10.1016/j.dsr2.2022.105223, 2023.

Lu, X., Yu, H., Ying, M., Zhao, B., Zhang, S., Lin, L., Bai, L., and Wan, R.: Western North Pacific Tropical Cyclone Database Created by the China Meteorological Administration, Adv. Atmos. Sci., 38, 690–699, doi:10.1007/s00376-020-0211-7, 2021.

Lu, X., Dong, C., Zhang, H., Lim Kam Sian, K. T. C., Yang, J., Xu, Z., Li, G., Wang, Q., Cao, Q., You, Z., and Sommeria, J.: Observational Analysis of Vertical Heat Flux Caused by Typhoon-Induced Near-Inertial Waves Under the Modulation of Mesoscale Eddies, J. Geophys. Res. Oceans, 129, e2024JC021053, doi:10.1029/2024jc021053, 2024.

Ma, Z., Fei, J., Lin, Y., and Huang, X.: Modulation of Clouds and Rainfall by Tropical Cyclone's Cold Wakes, Geophys. Res. Lett., 47, e2020GL088873, doi:10.1029/2020gl088873, 2020.

Nan, F., Xue, H., and Yu, F.: Kuroshio intrusion into the South China Sea: A review, Prog. Oceanogr., 137, 314–333, doi:10.1016/j.pocean.2014.05.012, 2015.

Qi, M., Han, B., Yang, Q., Wu, R., Liu, C., Zhang, G., Zhang, X., Zhou, H., Chen, J., and Chen, D.: Sea Surface Energy Fluxes' Response to the Quasi-Biweekly Oscillation: A Case Study in the South China Sea, Geophys. Res. Lett., 50, doi:10.1029/2023gl104288, 2023.

Quan, Q., Liu, Z., Yang, Y., Cai, Z., Zhang, H., and Liu, X.: Characterization of intraseasonal fluctuations in the abyssal South China Sea: An insight into the energy pathway, Prog. Oceanogr., 206, 102829, doi: 10.1016/j.pocean.2022.102829, 2022.

Shan, K., Chu, P.-S., and Yu, X.: Interdecadal Change of Tropical Cyclone Translation Speed during Peak Season in South China Sea: Observed Evidence, Model Results, and Possible Mechanism, J. Clim., 36, 4531–4541, doi:10.1175/jcli-d-

22-0704.1, 2023.

Song, X., Wang, X., Cai, W., and Xie, X.: Observed Air–Sea Turbulent Heat Flux Anomalies during the Onset of the South China Sea Summer Monsoon in 2021, Mon. Weather Rev., 151, 2443–2464, doi:10.1175/mwr-d-22-0314.1, 2023.

Tan, K., Xie, L., Bai, P., Zheng, Q., Li, J., Xu, Y., and Li, M.: Modulation Effects of Mesoscale Eddies on Sea Surface Wave Fields in the South China Sea Derived From a Wave Spectrometer Onboard the China-France Ocean Satellite, J. Geophys. Res. Oceans, 128, doi:10.1029/2021jc018088, 2023.

Wang, Q., Zhang, B., Zeng, L., He, Y., Wu, Z., and Chen, J.: Properties and Drivers of Marine Heat Waves in the Northern South China Sea, J. Phys. Oceanogr., 52, 917–927doi:10.1175/jpo-d-21-0236.1, 2022.

Wang, Q., Zeng, L., Shu, Y., Li, J., Chen, J., He, Y., Yao, J., Wang, D., and Zhou, W.: Energetic Topographic Rossby Waves in the northern South China Sea, J. Phys. Oceanogr., 49, 2697–2714, doi:10.1175/JPO-D-18-0247.1, 2019.

Wu, R., Zhang, H., and Chen, D.: Effect of Typhoon Kalmaegi (2014) on northern South China Sea explored using Muti-platform satellite and buoy observations data, Prog. Oceanogr., 180, 102218, doi:10.1016/j.pocean.2019.102218, 2020.

Xie, X., Liu, Q., Zhao, Z., Shang, X., Cai, S., Wang, D., and Chen, D.: Deep Sea Currents Driven by Breaking Internal Tides on the Continental Slope, Geophys. Res. Lett., 45, 6160–6166, doi:10.1029/2018GL078372, 2018.

Yang, Y., Wang, D., Wang, Q., Zeng, L., Xing, T., He, Y., Shu, Y., Chen, J., and Wang, Y.: Eddy-Induced Transport of Saline Kuroshio Water Into the Northern South China Sea, J. Geophys. Res. Oceans, 124, 6673–6687, doi:10.1029/2018jc014847, 2019.

Ying, M., Zhang, W., Yu, H., Lu, X., Feng, J., Fan, Y., Zhu, Y., and Chen, D.: An Overview of the China Meteorological Administration Tropical Cyclone Database, J. Atmos. Oceanic Tech., 31, 287–301, doi:10.1175/jtech-d-12-00119.1, 2014.

Zhang, H.: Modulation of Upper Ocean Vertical Temperature Structure and Heat Content by a Fast-Moving Tropical Cyclone, J. Phys. Oceanogr., 53, 493–508, doi:10.1175/JPO-D-22-0132.1, 2023.

Zhang, H., Chen, D., Tongya, L., Tian, D., He, M., Li, Q., Wei, G., and Liu, J.: A Moored Array Observation Dataset for Air-Sea·Surface, Upper and Bottom Ocean in the Northern South China Sea during 2014-2015 (MASCS 1.0) [Data set]. Zenodo. doi: 10.5281/zenodo.~~13827819~~13925651, 2024.

Zhang, H., Chen, D., Zhou, L., Liu, X., Ding, T., and Zhou, B.: Upper ocean response to typhoon Kalmaegi (2014), J. Geophys. Res. Oceans, 121, 6520–6535, doi:10.1002/2016jc012064, 2016.

Zhang, H., Liu, X., Wu, R., Chen, D., Zhang, D., Shang, X., Wang, Y., Song, X., Jin, W., Yu, L., Qi, Y., Tian, D., and Zhang, W.: Sea surface current response patterns to tropical cyclones, J. Marine Syst., 208, 103345, doi:10.1016/j.jmarsys.2020.103345, 2020.

Zhang, H., Wu, R., Chen, D., Liu, X., He, H., Tang, Y., Ke, D., Shen, Z., Li, J., Xie, J., Tian, D., Ming, J., Liu, F., Zhang, D., and Zhang, W.: Net Modulation of Upper Ocean Thermal Structure by Typhoon Kalmaegi (2014), J. Geophys. Res. Oceans, 123, 7154–7171, doi:10.1029/2018JC014119, 2018.

设置了格式: 英语(美国)